Sains Malaysiana 51(2)(2022): 533-546
http://doi.org/10.17576/jsm-2022-5102-17

Green Synthesis of Nickle Oxide Nanoparticles for Adsorption of Dyes

(Sintesis Hijau Nanozarah Nikel Oksida untuk Penjerapan Pewarna)

ISRAA MUZAHEM RASHID*, SAMI DAWOD SALMAN, ALAA KAREEM MOHAMMED & YASMIN SALIH MAHDI

ABSTRACT

The green synthesis of nickel oxide nanoparticles (NiO-NP) was investigated using $Ni(NO_3)_2$ as a precursor, olive tree leaves as a reducing agent, and D-sorbitol as a capping agent. The structural, optical, and morphology of the synthesized NiO-NP have been characterized using ultraviolet–visible spectroscopy (UV-Vis), X-ray crystallography (XRD) pattern, Fourier transform infrared spectroscopy (FT-IR) and scanning electron microscope (SEM) analysis. The SEM analysis showed that the nanoparticles have a spherical shape and highly crystalline as well as highly agglomerated and appear as cluster of nanoparticles with a size range of (30 to 65 nm). The Scherrer relation has been used to estimate the crystallite size of NiO-NP which has been found about 42 nm. The NiO-NPs have subsequently used as adsorbents for adsorption of two types of dyes; methylene blue (MB) as cation dye and methyl orange (MO) as anion dye. The removal efficiency of dyes from contaminated water was investigated during various key parameters at room temperature; initial dye concentration (Co), pH, contact time (t), agitation speed, and adsorbent dosage. The maximum removal of MB dye was found to be 96% (Co=25 mg/l, pH=10, contact time=100 min, agitation speed=300 rpm and adsorbent dosage=6 g/l), while for MO the maximum removal reached 88% at (Co=20 mg/L, pH=2, t =160 min, agitation speed=300 rpm and adsorbent dosage=6 g/L). The experimental adsorption data were found to well obey Freundlich isotherm. The kinetic investigation showed that the adsorption process for both dyes followed a pseudo-second-order model with rate constants 0.0109 and 0.0079 (mg/g min) for MB and MO, respectively.

Keywords: Adsorption; isotherm; kinetics; methyl orange; methylene blue; NiO nanoparticles; olive leaves

ABSTRAK

Sintesis hijau nanozarah nikel oksida (NiO-NP) telah dikaji menggunakan $Ni(NO_3)_2$ sebagai prakursor, daun pokok zaitun sebagai agen penurun dan D-sorbitol sebagai agen penutup. Struktur, optik dan morfologi NiO-NP yang disintesis telah dicirikan menggunakan analisis spektrofotometer ultralembayung-cahaya nampak (UV-Vis), pola pembelauan sinar-X (XRD), spektroskopi transformasi Fourier inframerah (FT-IR) dan mikroskop elektron imbasan (SEM). Analisis SEM menunjukkan bahawa nanozarah ini mempunyai bentuk sfera dan darjah hablur yang tinggi serta sangat beraglomerat dan ia hadir dalam gugusan dengan julat saiz daripada (30 hingga 65 nm). Hubungan Scherrer telah digunakan untuk anggaran saiz hablur NiO-NP yang telah dijumpai pada 42 nm. NiO-NP telah digunakan beberapa kali sebagai bahan penjerap untuk penjerapan dua jenis pewarna; metilena biru (MB) sebagai pewarna kation dan metil jingga (MO) sebagai pewarna anion. Kecekapan penyingkiran pewarna daripada air tercemar telah dikaji menggunakan beberapa parameter pada suhu bilik; permulaan kepekatan (Co) pewarna, pH, masa bertembung (t), kelajuan agitasi dan dos bahan penjerap. Penyingkiran pewarna MB maksimum yang telah dijumpai adalah 96% pada (Co=25 mg/l, pH=10, masa bertembung=100 min, kelajuan agitasi=300 rpm dan dos penjerap=6 g/l), manakala untuk MO nilai maksimum penyingkiran mencapai 88% pada (Co=20 mg/L, pH=2, masa bertembung=160 min, kelajuan agitasi=300 rpm and dos penjerap=6 g/L). Data uji kaji penjerap mendapati mengikuti model Freundlich. Kajian kinetik menunjukkan bahawa proses penjerapan untuk kedua-dua pewarna mengikuti model urutan kedua pseudo dengan kadar tetap 0.0109 dan 0.0079 (mg/g min) untuk masing-masing, iaitu MB dan MO.

Kata kunci: Daun zaitun; isoterma; kinetik; metilena biru; metil jingga; nanozarah NiO; penjerapan

INTRODUCTION

Nickel oxide nanoparticles have greatly attracted increasing attention because of their unique characteristics such as electrical, chemical and optical properties (Pelgrift & Friedman 2013; Sun et al. 2017). NiO-NPs have several applications in different fields. It is widely used as an electrochromic film, a magnetic material,

heterogeneous catalytic material, and battery electrode and as antibacterial/antifungal properties (Garb et al. 2019; Jing et al. 2018; Kingsley et al. 2018; Patel et al. 2017). Several chemical and physical methods have been carried out for the synthesis of NiO-NP including hydrothermal reaction (Chao et al. 2015), co-precipitation (Pooja & Dipali 2017), sol-gel (Zorkipli et al. 2016), polymer-matrix assisted synthesis (Anandan & Rajendran 2011), microemulsion (Han et al. 2016), and laser ablation (Olajire & Mohammed 2020). Although these methods may produce well defined pure nanoparticles but they have high cytotoxicity, low productivity, low antimicrobial activity, low antioxidant potential activity and are not environmental friendly (Kumar et al. 2019; Nagaraj et al. 2011). Furthermore, some of these techniques suffer from the difficulty in size homogeneity and dispersion of NiO nanoparticles.

Alternative to the chemical and physical methods are the green synthesis methods. These methods comprise using biological materials as reducing agents and capping agents such as plant extract, fungi, bacteria and algae (Salvadori et al. 2015; Shah et al. 2015). Plants are preferred in the bulk production of nanoparticles since they are readily available as well as its extract can easily be utilized in a much simple process (Asratemedhin & Mohammed 2020).

Green methods have been proposed as environmentally friendly since these methods generate environmentally benign products and by products (Miessya et al. 2019). Furthermore, the green methods are featured as cost-effective methods because of consuming less energy, eliminating the use of expensive chemicals and generating (Parveen et al. 2016). Synthesis of nanoparticle using plant extract is due to the presence of phytochemicals and different bioactive chemicals with various functional groups such as flavonoids, terpenoids, carboxylic acids, quinones, aldehydes, ketones, and amides (Bawazeer et al. 2021; Gulboy et al. 2015; Lingaraju et al. 2020). In the synthesis of the nanoparticles, these phytochemicals act as reducing agents which reduce the metal ions (in the metal salt as a precursor) into nano form by reduction mechanism (El Shafey 2020). The green synthesis of nickel oxide nanoparticle includes mainly three steps; selection of solvent medium (precursor), selection of biological source related reducing agent, selection of nontoxic stabilizing agents (Ezhilarasi et al. 2018, 2016). Different plants have been used for the synthesis of NiO-NP such as *Tamarix serotina* (Nasseri et al. 2016), *Moringa oleifera* (Ezhilarasi et al. 2016), *Agathosma betulina* (Thema et al. 2016). *Callistemon viminalis* (Sonea et al. 2016), and *Aegle marmelos* (Ezhilarasi et al. 2018). This study aims to prepare nickel oxide nanoparticles (NiO-NPs) using olive leave extract as reducing agent and D-sorbitol as stabilizing agent as well as examining the activity of these nanoparticles in removing of methyl orange and methylene blue dyes as contaminants from synthetic contaminated water.

Materials and Methods

Materials

Cationic dye MB, and anionic dye MO were purchased from Merck (Germany) with analytical grade. D-Sorbitol and nickel nitrate $Ni(NO_3)_2.6H_2O$ were purchased from BDH. Olive leaves were collected from farmer trees in the university of Baghdad, Iraq.

Preparation of $Ni(NO_3)_2$ solution

The solution of $Ni(NO_3)_2$ (10^{-3} M) was prepared by dissolving 0.029 g of salt $Ni(NO_3)_2.6H_2O$ in 100 mL deionized water.

Preparation of D-sorbitol solution

Sorbitol solution of (0.01 M) was prepared by dissolving 0.1821 g sorbitol in 100 mL deionized water.

Preparation of olive leaves extract (OLE)

The collected olive leaves (*Olea europaea*) were washed with distilled water for several times in order to remove any dust or insoluble particles. After that, these leaves were dried at 50 °C in an oven for 12 h to remove the residual moisture. Then, the dried leaves were cut into small pieces. In 1-L round bottomed Erlenmeyer flask, 120 g of leaves pieces were placed with 500 mL of sterile distilled water (Pandian et al. 2015). This mixture was heated in water bath at 65 °C for 3 h. Then after, the mixture is cooled at room temperature, filtered using Buchner funnel and filter paper (Whatman No.1). The filtration process was repeated several times (Marzieh & Rouhollah 2014). The aqueous extract solution was evaporated using a rotary evaporator to concentrate the extract by evaporating the largest possible amount of water. Then, the extract was put in the petri dish to be dried at room temperature. A stock solution of extract was prepared at concentrations 1.5 mg/mL.

Synthesis of NiO nanoparticles

For the synthesis of NiO-NP, 50 mL of $Ni(NO_3)_2$ (10^{-3} M) solution was mixed with 10 mL of olive leaves extract

(1.5 mg/mL) and 5 mL of sorbitol (10^{-2} M). The leaves extract acts as reducing agent while Sorbitol is used as a capping agent. At the beginning, the color of the mixture solution was light green. The mixture was stirred at 200 rpm in a water bath at 80 °C till the color is changed to dark grey. Then after, the solution is centrifuged at 10000 rpm for 30 min (Rahdar et al. 2015). The supernatant was thrown out while the nanoparticles were washed with sterile deionized water and centrifuged again at 10000 rpm for 10 min to remove the residue particles that were not the capping agent. The participated particles were washed with deionized water, dried at 60 °C for 4 h and calcined at 500 °C for 5 h (Javed et al. 2019). Then, the NiO nanoparticles were collected as blackish grey powder. This powder was kept in an air tight container for further use.

CHARACTERIZATION OF NIO-NP

The prepared samples of NiO-NP have been characterized by measuring the absorption spectra using double beam UV-VIS Spectrophotometer (PG Instruments, Model UV T80, England) from 200 to 800 nm. The morphology of the prepared sample of NiO-NP nanoparticles was examined using a Scanning Electron Microscope SEM analysis (JEOL Jsm-6480 LV). X-ray diffraction XRD (Shimadzu XRD6000) was used at scanning rate 20 °C/min in a 2θ range from (30 -85) to study the structural information and crystalline size of NiO-NP. Fourier transform infrared (FT-IR) analysis, using IR Prestige-21 Shimadzu, was implemented to characterize the functional groups on the surface of the NiO-NP. The scanned spectra were in the range 400 - 4000 cm^{-1} at a resolution of 4 cm^{-1}.

ADSORPTION EFFICIENCY OF NiO-NP

The adsorption efficiency of the prepared NiO-NP was examined for two types of dyes; one was cationic MO dye, and the other was anionic MB dye using batch experiments. In these experiments, a specific amount of NiO-NP was added to 100 mL of a synthetic solution of MO and MB separately. The initial concentration of the dye solution was 100 ppm. The mixture was shaken using a thermostatic shaker (Edmund Buhler SM25, German). The parameters studied during the batch experiments contact time (0 - 220 min), pH (2 - 12), mixing speed (0 - 400), sorbent dosage (1 - 10 g/L) and dye initial concentration (5 - 40 ppm). Sample (25 mL) of each solution is withdrawn from each flask, filtered using syringe filter (20 μm) in order to separate the adsorbent from the aqueous solution. The concentration of the remaining dye in the filtered solution was analyzed using a double beam UV-visible spectrophotometer (PG Instruments, Model UV T80, England). The UV-Vis analysis was implemented at λ_{max} = 484 nm for MO and at λ_{max} = 516 nm for MB. The removal efficiency (R%) of the dye onto NiO-NP was calculated using (1) (Huang et al. 2017):

$$R\% = \frac{(C_o - C_e)}{C_o} \times 100 \quad (1)$$

where C_o is the initial dye concentration and C_e is the concentration of the dye after reaching the equilibrium. The quantity of the dye adsorbed by the NiO-NP has been determined using equation (2) (Huang et al. 2017):

$$q_e = \frac{(C_o - C_e)V}{m} \quad (2)$$

where q_e (mg/g) is the quantity of the dye adsorbed per gram of the nanoparticles; V (mL) is the volume of the sample; and m (g) is the quantity of the adsorbent NiO-NP added.

ADSORPTION ISOTHERMS

Adsorption isotherms are models that relate adsorbate removal per unit mass of sorbent, q_e, to the equilibrium sorbate concentration in the bulk solution phase, C_e. These models are usually based on different assumptions related to the possibility of interaction between sorbate species, type of coverage and the homogeneity/heterogeneity of the sorbents (Elmorsi 2011; Hamdaoui & Naffrechoux 2007). The linearized forms of Langmuir and Freundlich isotherms (represented by equations (3) and (4), respectively, are used to describe the adsorption process:

$$\frac{1}{q_e} = \frac{1}{q_m} + \frac{1}{q_m K_L}\frac{1}{C_e} \quad (3)$$

$$lnq_e = lnK_F + \frac{1}{N} lnC_e \quad (4)$$

ADSORPTION KINETICS

Adsorption kinetics study has been carried out using pseudo-first-order and pseudo-second-order models (Guechi & Hamdaoui 2016; Lim 2017). The pseudo first-order rate expression is given by (5):

$$\left(\frac{dq_t}{dt}\right) = K_1(q_e - q_t) \quad (5)$$

The linearized form of pseudo-first-order rate is given by (6):

$$ln\ ln\ (q_e - q_t) = ln\ ln\ q_e - k_1 t \quad (6)$$

where q_e is the amount of dye adsorbed by adsorbate(NiO-NPs) at equilibrium(mg/g); q_t is the amount of dye adsorbed at time, t; k_1 is the first-order rate constant (min^{-1}).

A plot of $ln\ ln\ (q_e - q_t)$ versus t gives a linear relationship from which qe and k_1 can be determined from slope and intercept. The pseudo-second-order rate is expressed in (7):

$$\frac{dq}{dt} = k_2(q_e - q_t)^2 \quad (7)$$

The linearized form of pseudo-second-order rate is given by (8):

$$\frac{t}{q_t} = \left(\frac{1}{k_2 q_e^2}\right) + \left(\frac{t}{q_e}\right) \quad (8)$$

where k_2 is the pseudo second-order rate constant (g/mg min).

A plot of t/q_t versus t gives a linear relationship, from which q_e and k_2 can be determined from the slope and intercept.

Results and Discussion

Characterization of NIO-NP

Characterization by UV-Vis Spectroscopy

The absorption spectra of the prepared NiO-NP were examined using a UV-Visible spectrophotometer. Figure 1 shows that NiO-NPs has a maximum absorbance at a wavelength 324 nm. This result is in agreement with that mention by Miessya et al. (2019). The olive leaves extract has absorbance spectra at a maximum wavelength of 270 nm (El-Kemary et al. 2013) while the precursor $Ni(NO_3)_2$ has a maximum wavelength at 302 and 391 nm. The unique optical properties of NiO-NP are due to the property of surface Plasmon resonance (SPR) (Infantiya et al. 2020).

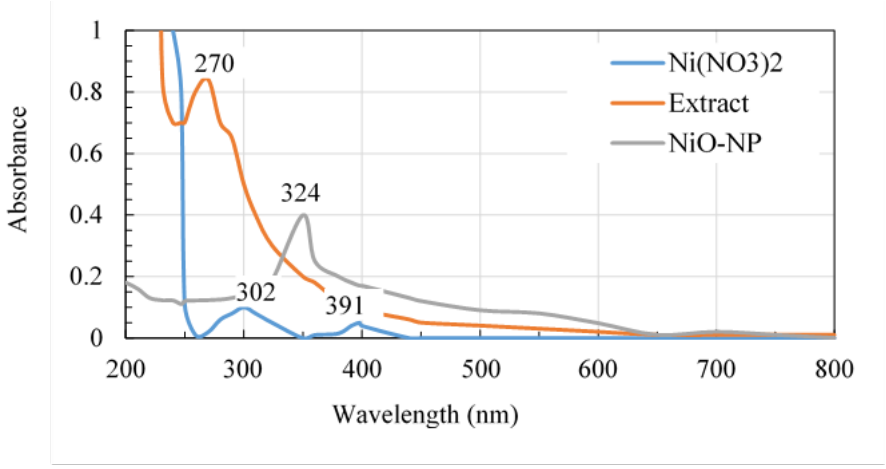

FIGURE 1. Absorption spectra of $Ni(NO_3)_2$, olive leaves extract, and NiO-NP

Characterization using FTIR

The green-synthesized NiO-NP was characterized using the FTIR spectrum to investigate the functional groups of olive leaves extract. Figure 2 shows the spectrum of olive leaves extract and the prepared NiO-NP. The FTIR analysis olive leaves extract shows a number of absorption peaks. A peak at 2935 cm^{-1} observed due to –CH stretching vibrations of $–CH_3$ and $–CH_2$ functional groups. The peak at 3383 cm^{-1} refers to the stretching bond of N-H of the amino group. Peaks at 338 and 1705 cm^{-1} indicates C=O and O-H groups stretching. The fingerprint region of O-H, CO, and C-O was indicated at the peak 1604 cm^{-1} which represents the functional groups of olive leaves extract (Gulboy et al. 2016). While the FTIR analysis of NiO-NPs exhibits amine (N-H), hydroxyl (-OH), and the carboxyl (-C=O) which indicates that the olive leaves extract was mainly involved in the reduction of Ni^{+2} to Ni^0 nanoparticles. The FTIR spectrum of the prepared NiO-NPs is shown in Figure 2. The peak located at 3441 cm^{-1} belongs to the hydroxyl group O-H stretching vibrations

which are generally carboxylic acids and phenolics (Infantiya et al. 2020). The peaks at 1462, 1388, 1112, and 1037 cm^{-1} belong to the oxide groups. The characteristic peak at 452 cm^{-1} attributes to the Ni-O vibration. Thus, it is clearly indicating that the phytochemicals from plant materials act as reducing agent during the formation of nanoparticles (Lingaraju et al. 2020).

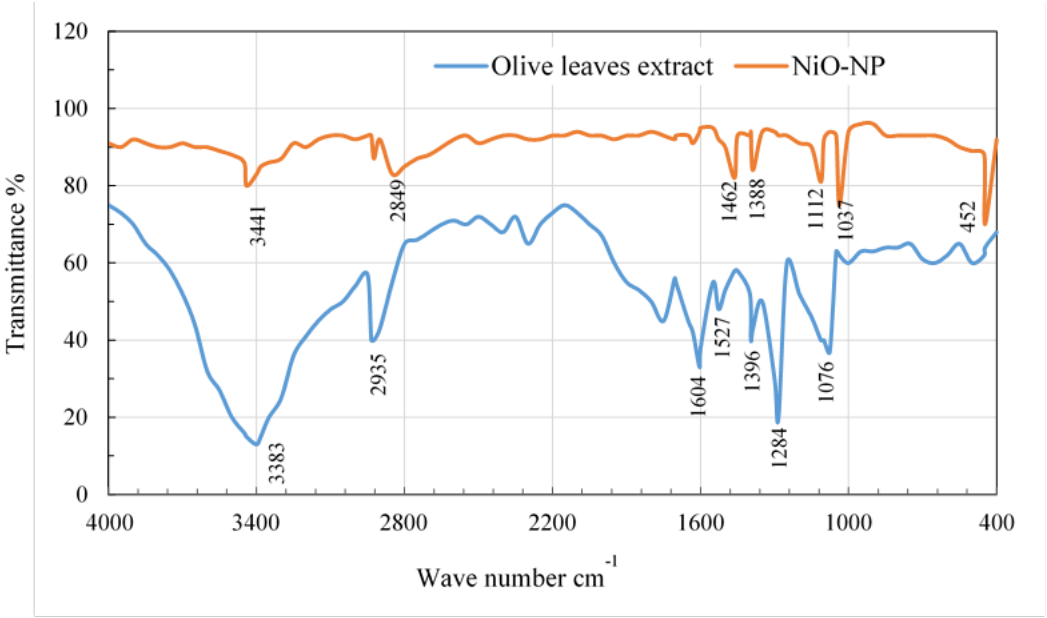

FIGURE 2. FTIR analysis of olive leaves extract and NiO-NP

XRD ANALYSIS

X-ray diffraction was used to study the structural information and crystalline size of NiO-NP. Figure 3 shows five-strong intense peaks at 2θ of 37.18, 43.095,62.62, 75.24, and 79.185°. The diffracting planes of the NiO crystallites are 111, 200, 220, 311 and 222. These reflections show that the formed nanoparticles have crystalline structure of face centered cubic (fcc), the lattice constant which agrees with standard data of (JCPDScardno.47-1049). The Debye–Scherrer's formula (Mariam et al. 2014) equation (9) was used to estimate the crystallite size which has been found in the range 30-65 nm:

$$D = \frac{K\,\lambda}{\beta\ Cos\ \theta} \tag{9}$$

where λ is the wavelength of the x-ray (1.5405 Å); θ is the angular position of the peak; K is an empirical constant equal to 0.9 and β is the full width at half maximum of the diffraction peak. The crystallite sizes of NiO samples is 42 nm which was calculated from measured values for the spacing of the (111) plane.

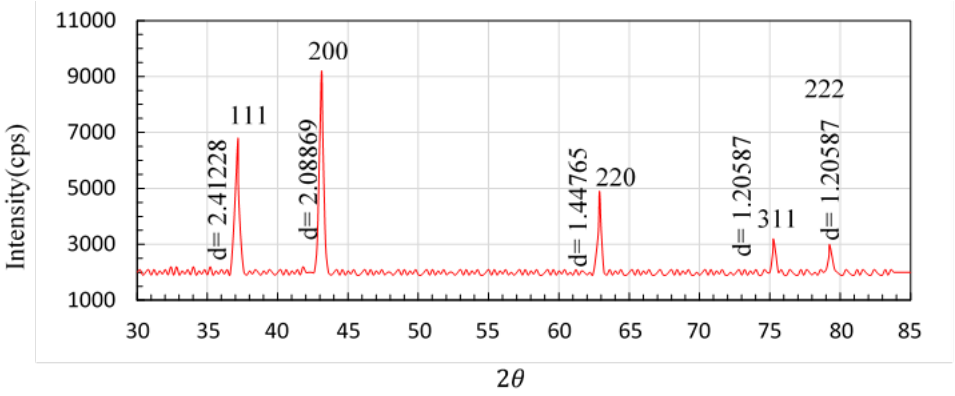

FIGURE 3. XRD pattern of NiO-NP

SEM ANALYSIS

SEM analysis was used to study the morphological features of nickel oxide nanostructures. Figure 4 shows the SEM image of the prepared NiO-NPs with a magnification of 10 kV. The image shows that the nanoparticles have a spherical shape and highly crystalline as well as highly agglomerated and appear as cluster of nanoparticles with a size range of 30 to 65 nm with average crystalline size of about 42 nm. The agglomeration of nanoparticles may be due to the exposure of the particles to large volume of heat during calcination step (Saiganesh et al. 2020) or because of the high surface tension of the ultrafine nanoparticles and high surface energy (Kamiya et al. 2018). The SEM analysis result is compatible with the results of (Pooyandeh et al. 2020) who study the morphology of NiO nanoparticles which prepared by the sol-gel method using two different precursors nickel chloride hexahydrate and nickel nitrate hexahydrate.

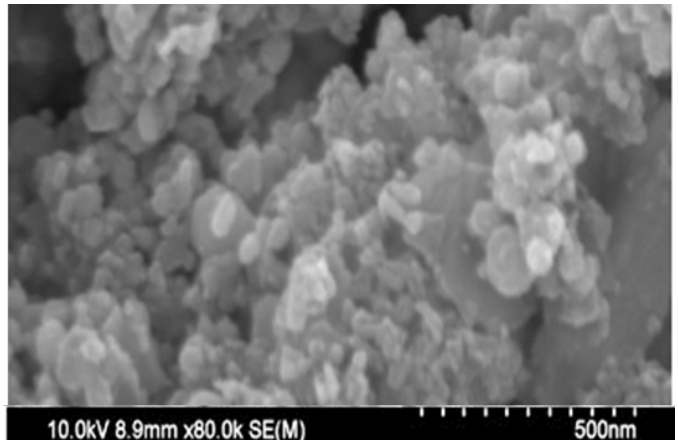

FIGURE 4. SEM image of NiO nanoparticle after calcination

BATCH EXPERIMENTS OF DYES REMOVAL

CONTACT TIME

The contact time is an essential parameter in the adsorption process, since it determines the necessary time needed to achieve the equilibrium in the adsorption process. Furthermore, the contact time predicts the feasibility of the adsorbent for its use in the adsorption system. The effect of contact time on the removal efficiency was studied using different values of contact time (0-220 min). The values of other parameters were fixed (initial dye concentration Co = 100 ppm, pH = 7, agitation speed = 200 rpm, and adsorbent dose = 1g/L). Figure 5 shows that the removal efficiency increased with increasing the contact time until a certain value after which the percent removal became constant. Maximum removal 79% of MB dye was obtained at contact time 100 min, while maximum removal 38% of methyl orange MO was obtained at 160 min. At the initial stages of sorption stages, the sorption rate was rapid because greater number of active sites are available on the surface of the adsorbent. As time passes, the number of these active sites begins to decrease and hence fixe the adsorption process (Basma et al. 2017). The results of contact time are consistent with that mentioned by Khatem et al.

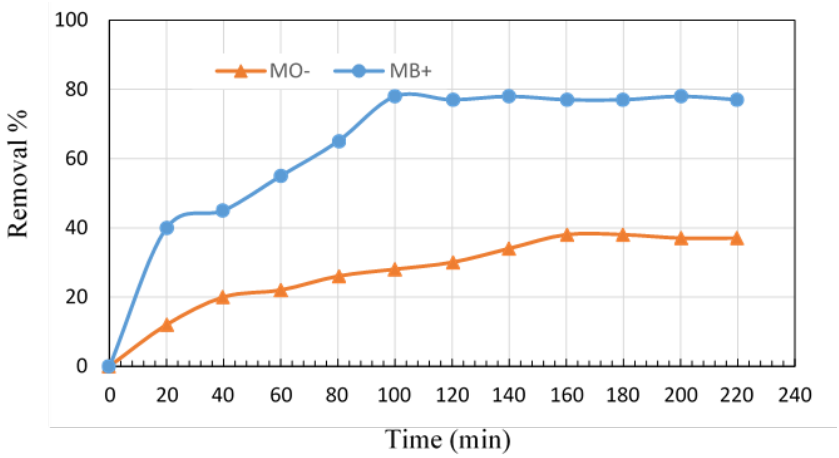

FIGURE 5. Effect of time on adsorption capacity

(Co = 100 ppm, pH = 7, agitation speed = 200 rpm, and adsorbent dose = 1g/L)

(2015) who studied the adsorption of diclofenac (anti-inflammatory) on hydrotalcite synthetic clay and on its calcined product. They found that the equilibrium was reached after 50 min of contact time.

INITIAL pH OF THE SOLUTION

The acidity of the solution plays an important role in the sorption process. The removal efficiency of the dyes was examined at different values of pH ranging from 2 to 12. Other parameter values were kept constant (Co = 100 ppm, rpm =2 00, adsorbent dose = 1g/L and t = 100 min for MB and contact time = 160 min for MO). The initial value of the solution pH was adjusted using 0.1 M NaOH and 0.1 M HCL. Figure 6 shows that increasing the value of pH leads to an increase in the percent removal of MB and reaches 87% at pH = 12. This behavior can be interpreted as follows, increasing the value of pH leads to an increase in the negative charges on the surface of the NiO-NP, this negatively charged surface will enhance the attractive forces with the positively charged cation of MB dye which in turn increases the uptake of the MB dye on the adsorbent nanoparticles. This behavior is in agreement with the result obtained by Al-Aoh (2018) who studied the adsorption of bromophenol blue dye (BB) on the nickel oxide nanoparticles. He noticed that the uptake of BB increases with increasing the value of pH and attributed that due to the electrostatic attraction forces between the negative charges on the surface of the adsorbent and the positive charges of the cation adsorbate BB dye. For MO dye, increasing the value of the pH leads to decrease the percent removal of the dye. The reason for this belongs to the repulsion forces between the negatively charged of the adsorbent surface and the anionic MO dye adsorbent. The percent removal of MO reaches about 29% when pH increased to 12. This finding is consistent with that found by Barzinjy et al. (2020) who studied the adsorption of methyl orange dye on NiO-NPs that prepared using antioxidant content

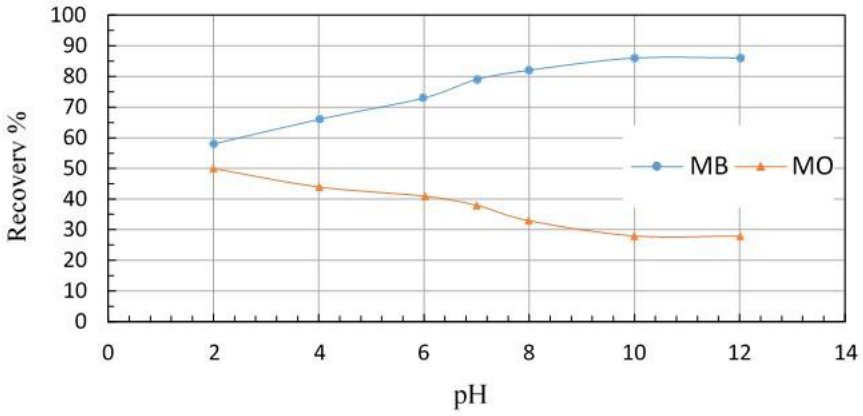

FIGURE 6. Effect of pH on adsorption capacity
(Co = 100 ppm, agitation speed = 200 rpm, adsorbent dose = 1g/L, and contact time =100 min for MB, and t = 160 min for MO)

of *Punica granatum* L. (pomegranate) juice extract as reducing agent. They noticed that increasing the value pf pH results in decreasing the uptake of the dye by the adsorbent. They attributed that to the electrostatic repulsion forces between the negatively charges of both the adsorbent surface and adsorbate.

AGITATION SPEED

The effect of agitation speed on the uptake of dyes was studied by varying the agitation speed in the range of 0 - 400 rpm. The other parameters are kept constant (Co = 100 ppm, contact time =100 min for MB and 160 min for MO, adsorbent dose =1 g/L pH = 10 for MB and 2 for MO. Figure 7 shows that the removal percent of dyes by NiO-NP is increased with increasing the value of agitation speed from 0 to 300 rpm after which there is no significant improvement in the recovery efficiency. Both dyes show a maximum percent removal at 300 rpm and equal to 92 and 65% for MB and MO dye, respectively. Increasing agitation speed will reduce the diffusion resistance of the liquid film that surrounding the surface of the adsorbed solid and hence facilitates proper contact between the dye solution and the active sites on the solid adsorbed. Agitation higher than 300 rpm has no significant effect on the uptake of the dyes.

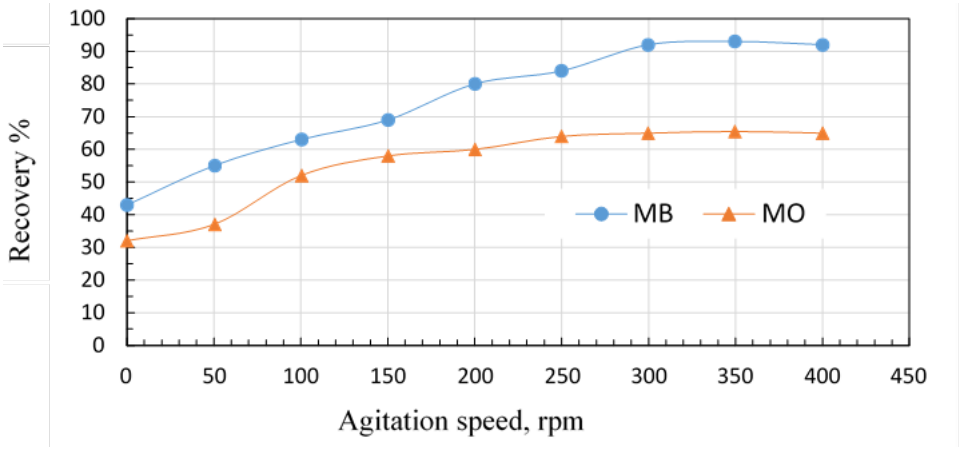

FIGURE 7. Effect of mixing speed on removal efficiency

(Co = 100 ppm, pH = 10 for MB and pH = 2 for MO, adsorbent dose = 1g/L, and contact time = 100 min for MB and t = 160 min for MO)

The behavior of agitation effect is consistent with the results obtained by Abdulkareem and Anwer (2021) who studied the adsorption of different dyes on micro algal dry biomass. They showed that maximum uptake of dyes occurs at 150 rpm after which there was no improvement in the adsorption efficiency. These results are consistent with Priyadarshini et al. (2018) and Raval et al. (2016).

NiO-NP DOSAGE

In order to show the effect of NiO-NP dose on the removal of dyes from the contaminated solution, different values of adsorbent dose were used in the range of 1 - 10 g/L. The other parameters are kept constant (Co =100 ppm, contact time =100 min for MB and 160 min for MO, pH =10 for MB and 2 for MO and agitation speed = 300 rpm). Figure 8 shows that the removal efficiency was

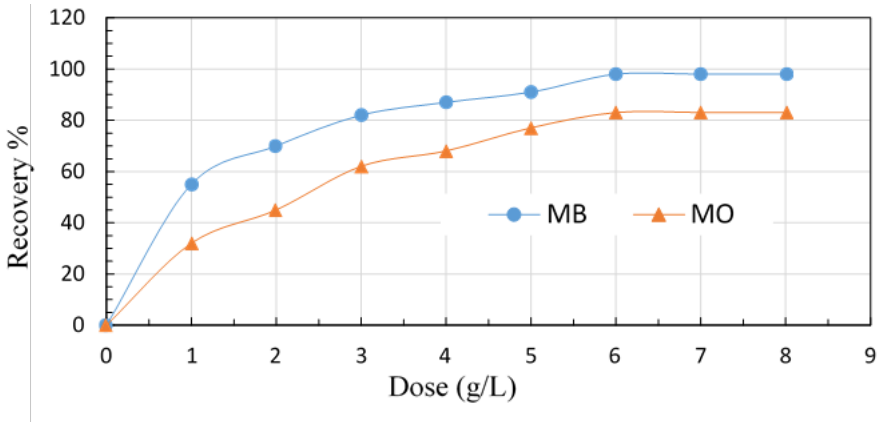

FIGURE 8. Effect of adsorbent dosage on removal efficiency

(Co = 100 ppm, contact time t = 100 min for MB and 160 min for MO, pH = 10 for MB and pH = 2 for MO, and agitation speed = 300 rpm)

increased with increasing the adsorbent dosage until a certain value after which the removal remains constant. The best value of adsorbent dosage is 6 g/L of solution. Increasing the adsorbent dosage in the solution means increasing the availability of the sorption sites, therefore, the uptake of the dyes increased. After a certain value of the adsorbent dosage, the maximum removal sets in because sufficient amount of the dyes will bound to the surface of the adsorbent and no more adsorption occurs even with further increasing the adsorbent dosage. These results are in agreement with Kankeu et al. (2016).

INITIAL DYE CONCENTRATION

For studying the effect of the initial dye concentration, experiments were carried out by varying the values of initial dye concentration within the range of 5 - 40 mg/L at intervals of 5 mg/L for both dyes. The experiments related to MB were carried out at optimized values: pH = 10 and time of mixing 100 min NiO-NP dose 6 g/L and mixing speed 300 rpm. While for MO dye, the experiments were carried out at optimized values: pH = 2 and time of mixing 160 min NiO-NP dose 6 g/L and mixing speed 300 rpm. Figure 9 shows that at low values of initial dye concentration, the removal efficiency is low, this is because, at a lower concentration, the number of active sites on the adsorbent surface is more than the dye molecules number. The removal efficiency increases with increasing the initial concentration till a certain value after which the removal efficiency begins to decrease. This behavior can be interpreted as; at high concentrations, there are no sufficient active sites that available in the nanoparticles for more adsorption of dye molecules (Khoshhesab & Ahmadi 2016; Kuang et al. 2020). Figure 9 shows that for MB dye, the maximum removal (96%) occurs at initial concentration Co = 25 mg/L, while for MO dye, the maximum removal (88% occurs at Co = 20 mg/L).

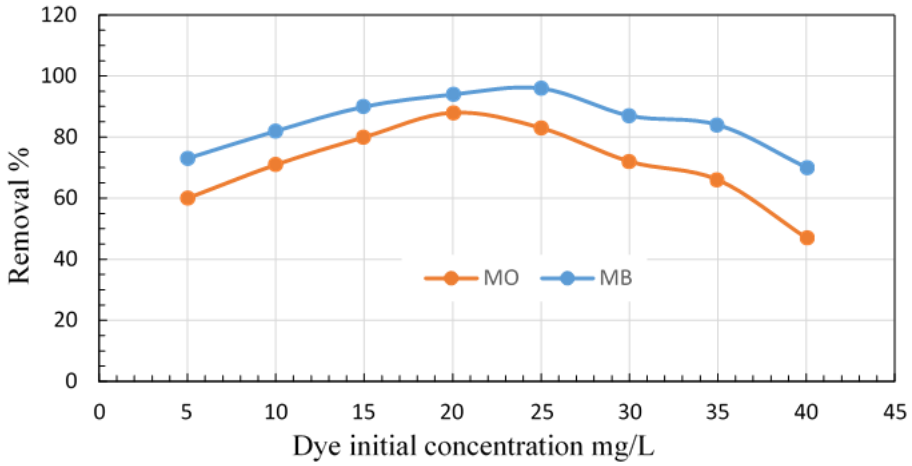

FIGURE 9. Effect of dye initial concentration on removal efficiency, mixing speed 300 rpm, NiO-NP dose 6 g/L, time = 100 min for MB and 160 min for MO, pH = 10 for MB and 2 for MO

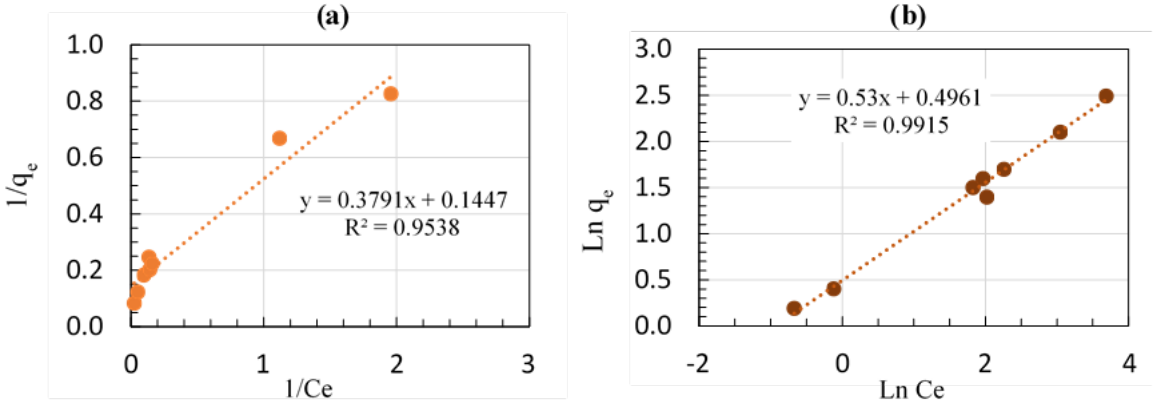

FIGURE 10. Linear form of isotherm models for sorption of MO dye onto NiO-NP: (a) Langmuir, and (b) Freundlich

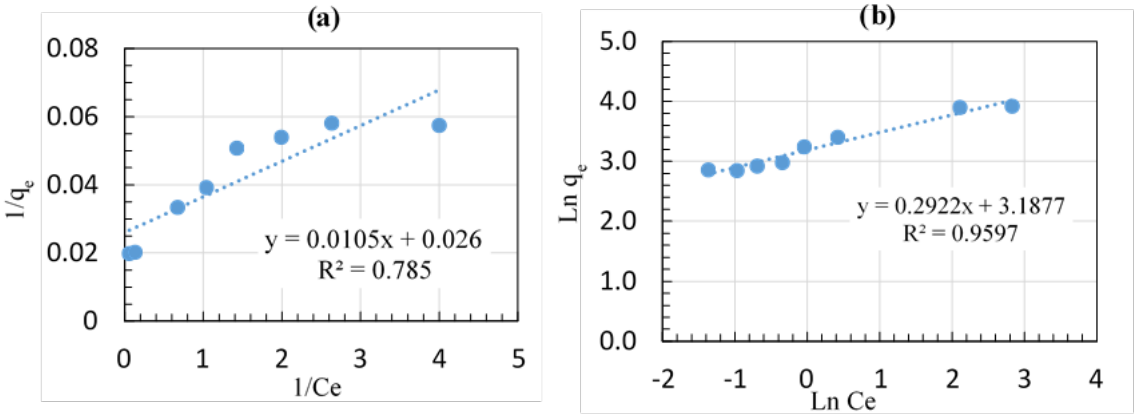

FIGURE 11. Linear form of isotherm models for sorption of MB dye onto NiO-NP: (a) Langmuir and (b) Freundlich

ADSORPTION ISOTHERMS

For a clear examination of the relationship between amount of MO and MB dyes adsorbed and their concentration, Langmuir, Freundlich isothermal models were used. Figures 10 and 11 show the fitting of the adsorption data with linearized form of the two isotherms. The assessment of the models was based on the values of the correlation coefficients R^2.

Table 1 shows the empirical coefficients for each model which is determined from the slope and intercept of the linear plot using Microsoft Excel 2016 software. The R^2 values of the Freundlich model were greater than that of the Langmuir model for the adsorption of the both dyes; MB and MO dyes. This indicates that the adsorption of both dyes on NiO-NP particles is better described by the Freundlich than Langmuir model.

TABLE 1. Langmuir and Freundlich parameters for adsorption of MB and MO on NiO-NPs

Adsorbate	Langmuir			Freundlich		
	K_L	q_m	R^2	K_F	N	R^2
MB	2.476	38.46	0.785	24.23	3.422	0.9597
MO	0.3817	6.91	0.953	1.642	1.88	0.9915

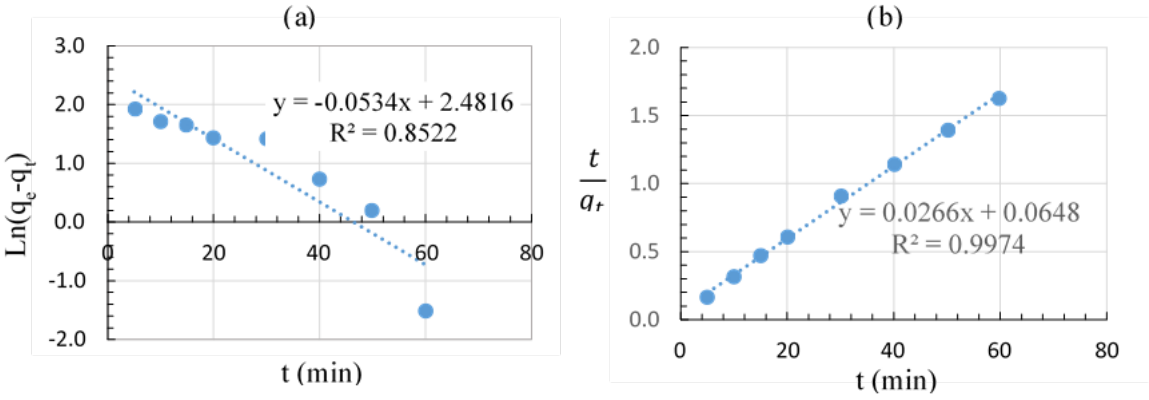

FIGURE 12. (a) Pseudo-first-order, and (b) Pseudo-second-order kinetics models for adsorption of MB dye onto NiO-NPs

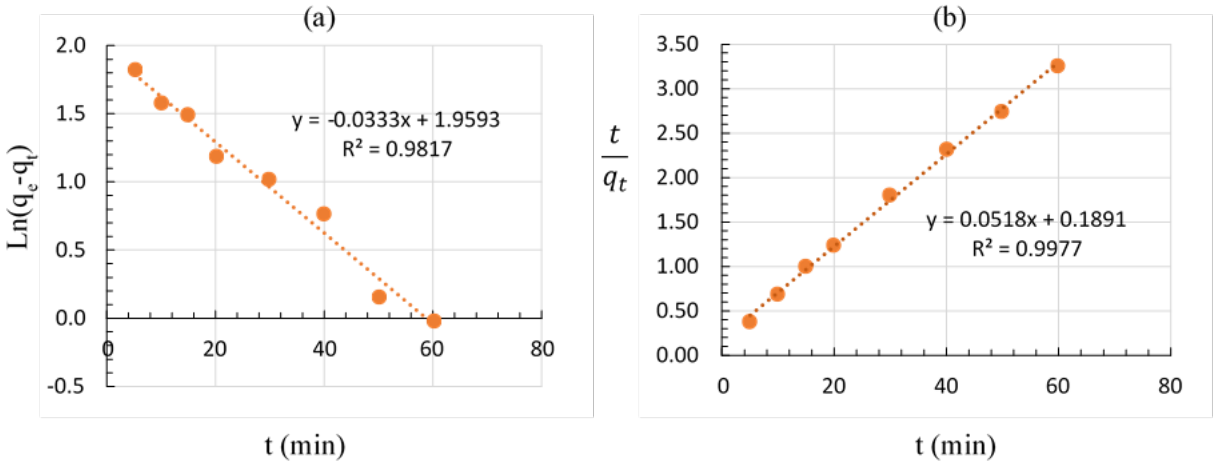

FIGURE 13. (a) Pseudo-first-order, and (b) pseudo-second-order kinetics models for adsorption of MO dye onto NiO-NPs

ADSORPTION KINETICS

The rate of removal of MO and MB dyes and its controlling mechanism fitted to pseudo first and pseudo second-order kinetic models to describe MO and MB dyes uptake onto NiO-NPs. The parameters for each model were obtained by fitting the linearized form of these models to the experimental data as shown in Figures 12 and 13.

Table 2 shows the correlation coefficients (R^2) and all parameters determined from the slope and intercept of the linear plot using Microsoft Excel 2016 software. It is clear from Figures 12 and 13 and Table 2 that the sorption of two dyes is likely to be second-order because the value of q_e (experimental) was closer to q_e (calculated) for the second-order model than the first-order model, as well as the values of R^2 of pseudo second order is higher than that of pseudo-first order. These results show that the chemosorption mechanisms have been dominant in dyes sorption on NiO-NPs. These results are in agreement with that found by Serpil and Mehmet (2017).

TABLE 2. Pseudo-first-order and Pseudo-second-order kinetic model for MB and MO dyes adsorption onto NiO-NPs

Kinetic model	Parameter	MB	MO
Pseudo-first-order	k_1 (min^{-1})	0.0534	0.0333
	q_e (experimental, mg/g)	37.11	19.4
	q_e (calculated, mg/g)	11.96	7.09
	R^2	0.8522	0.9817
Pseudo-second-order	k_2 (mg/g min)	0.0109	0.0079
	q_e (experimental, mg/g)	37.11	19.4
	q_e (calculated, mg/g)	37.59	19.3
	R^2	0.9974	0.9977

Conclusion

Nickel oxide nanoparticles can be synthesized using olive leaves extract as a reducing agent and sorbitol D as a capping agent. The crystallite size distribution of the prepared NiO-NPs was found to be in the range of 30 to 65 nm. The average size of the NiO nanoparticle observed from SEM images is 42 nm. Maximum percent removal of MB dye was 96% which occurs at the best conditions (contact time = 100 min, pH=10, agitation speed 300 rpm, adsorbent dosage =6 g/Land Co=25 ppm). While for methyl orange, the maximum removal percent was 88% at optimum conditions (contact time = 160 min, pH = 2, agitation speed 300 rpm, adsorbent dosage = 6 g/L and Co = 20 ppm). The adsorption data for both dyes MB and MO were well fitted by the Freundlich isotherm model with correlation coefficients (R^2) equal to 0.9597 and 0.9915, respectively. The kinetics study showed that the adsorption process of both dyes obeyed pseudo-second-order rate model with rate constants for methylene blue, and for methyl orange. This result proved that the chemosorption has been predominant in the sorption of dyes on the nickel oxide nanoparticles.

Acknowledgements

Special gratitude to the University of Baghdad AL Khwarizmi College of Engineering for the offered assistance to carrying out this investigation.

References

Abdulkareem, P.M. & Anwer, S.S. 2021. Uptake of different dyes by two new strains of microalgal dry biomass. *Iraqi Journal of Agricultural Sciences* 52(1): 48-62.

Al-Aoh, H.A. 2018. Adsorption performances of nickel oxide nanoparticles (NiO NPs) towards bromophenol blue dye (BB). *Desalination and Water Treatment* 110: 229-238.

Anandan, K. & Rajendran, V. 2011. Morphological and size effects of NiO nanoparticles via solvothermal process and their optical properties. *Materials Science in Semiconductor Processing* 14(1): 43-47.

Asratemedhin, B.H. & Mohammed, O. 2020. Plant extract mediated synthesis of nickel oxide nanoparticles. *Progress in Materials Science* 2(2): 0205-0209.

Barzinjy, A.A., Hamad, S.M., Esmaeel, M.M., Aydin, S.K. & Hussain, F.H. 2020. Biosynthesis and characterisation of zinc oxide nanoparticles from *Punica granatum* (pomegranate) juice extract and its application in thin films preparation by spin-coating method. *Micro and Nano Letters* 15(6): 415-420.

Basma, A.A., Raheem, J.M. & Nawras, J.J. 2017. Adsorption of mefenamic acid from water by bentonite poly urea formaldehyde composite adsorbent. *Journal of Engineering* 23(7): 50-73.

Bawazeer, S., Abdur, R., Syed, S., Uzair, A., Shawky, A.M., Al-Awthan, Y.S., Bahattab, O.S., Uddin, G., Sabir, J. & El-Esawi, M.A. 2021. Green synthesis of silver nanoparticles using *Tropaeolum majus*: Phytochemical screening and antibacterial studies. *Green Processing and Synthesis* 10(1): 85-94.

Chao, W., Dipali, S., Fengbo, T., Yuncai, L., Shudi Peng, Wei, S. & Qu, Z. 2015. Hydrothermal synthesis and structural characterization of NiO/SnO_2 composites and hydrogen sensing properties. *Journal of Spectroscopy* 2015: Article ID. 450485.

El Shafey, A.M. 2020. Green synthesis of metal and metal oxide nanoparticles from plant leaf extracts and their applications: A review. *Green Processing and Synthesis* 9(1): 304-339.

Elmorsi, T.M. 2011. Equilibrium isotherms and kinetic studies of removal of methylene blue dye by adsorption onto miswak leaves as a natural adsorbent. *Journal of Environmental Protection* 2(6): 817-827.

El-Kemary, M., Nagy, N. & El-Mehasseb, I. 2013. Nickel oxide nanoparticles: Synthesis and spectral studies of interactions with glucose. *Materials Science in Semiconductor Processing* 16(6): 1747-1752.

Ezhilarasi, A.A., Vijava, J.J., Kaviyarasu, K. & Maaza, M.A. 2016. Green synthesis of NiO nanoparticles using *Moringa oleifera* extract and their biomedical applications: Cytotoxicity effect of nanoparticles against HT-29 cancer cells. *Journal of Photochemistry and Photobiology B: Biology* 164: 352-360.

Ezhilarasi, A.A., Judith, J.V. & Kaviyarasu, K. 2018. Green synthesis of NiO nanoparticles using *Aegle marmelos* leaf extract for the evaluation of *in-vitro* cytotoxicity, antibacterial and photocatalytic properties. *Journal of Photochemistry and Photobiology B: Biology* 180: 39-50.

Garb, D.S., Abu Baker, Y. & Suleiman, S. 2019. Nickel oxide (NiO) devices and applications: A review. *International Journal of Engineering Research and Technology* 8(4): 461-467.

Guechi, E.K. & Hamdaoui, O. 2016. Biosorption of methylene blue from aqueous solution by potato (*Solanum tuberosum*) peel: Equilibrium modelling, kinetic, and thermodynamic studies. *Desalination and Water Treatment* 57(22): 10270-10285.

Gulboy, A.N., Alaa, K.M. & Hasan, F.S. 2016. Biosynthesis and characterization of silver nanoparticles using olive leaves extract and sorbitol. *Iraqi Journal of Biotechnology* 15(1): 22-32.

Gulboy, A.N., Alaa, K.M. & Hasan, F.S. 2015. Effects of silver nanoparticles in liver function and oxidative stress levels. *World Journal of Pharmaceutical Research* 4(9): 2080-2089.

Hamdaoui, O. & Naffrechoux, E. 2007. Modeling of adsorption isotherms of phenol and chlorophenols onto granular activated carbon. Part 1. Two-parameter models and equations allowing determination of thermodynamic parameters. *Journal of Hazardous Materials* 147: 381-394.

Han, D.Y., Wang, C.Q., Li, D.D. & Cao, Z.B. 2016. NiO/ZnO core-shell nanoparticles *in situ* synthesis via microemulsion method. *Synthesis and Reactivity in Inorganic, Metal-Organic, and Nano-Metal Chemistry* 46(5): 794-797.

Huang, Z., Li, Y., Chen, W., Shi, J., Zhang, N., Wang, X., Li, Z., Gao, L. & Zhang, Y. 2017. Modified bentonite adsorption of organic pollutants of dye wastewater. *Material Chemistry and Physics* 202: 266-276.

Infantiya, S.G., Vinola, J. & Subramanian, D. 2020. Synthesis and characterization of nickel oxide nano particles by sol-gel technique. In *AIP Conference Proceedings*. AIP. 070017.

Javed, I., Ahsan, A., Tariq, M. & Safia, H. 2019. Green synthesis and characterizations of nickel oxide nanoparticles using leaf extract of *Rhamnus virgata* and their potential biological applications. *Applied Organometallic Chemistry* 33(8): 4950.

Jing, M., Wen, L., Shuyuan, Z., Zhe, M., Peishuai, S., Fuhua, Y. & Xiaodong, W. 2018. A thin film flexible super capacitor based on oblique angle deposited Ni/NiO nanowire arrays. *Nanomaterials* 8(422): 1-10.

Kamiya, H., Yoshio, O., Masayoshi, F. & Minoru, M. 2018. Characteristics and behavior of nanoparticles and its dispersion systems. In *Nanoparticle Technology Handbook*, edited by Naito, M., Yokoyama, T., Hosokawa, K. & Nogi, K. Amsterdam: Elsevier. pp. 109-168.

Kankeu, E.F., Waanders, F., Charissa, L.F. & Laurette, F. 2016. Adsorption of congo red by surfactant-impregnated bentonite clay. *Desalination and Water Treatment* 57(57): 27663-27671.

Khatem, R., Ojeda, R. & Bakhti, A. 2015. Use of synthetic clay for removal of diclofenac anti-inflammatory. *Eurasian Journal of Soil Science* 4(2): 1-11.

Khoshhesab, Z.M. & Ahmadi, M. 2016. Removal of reactive blue 19 from aqueous solutions using NiO nanoparticles: Equilibrium and kinetic studies. *Desalination and Water Treatment* 57(42): 20037-20048.

Kingsley, O.U., Freddie, L.I. & Andrew, C.E. 2018. Fabrication of affordable and sustainable solar cells using NiO/TiO_2 *P-N* heterojunction. *International Journal of Photoenergy* 2018: Article ID. 6062390.

Kuang, Y., Xiaoping, Z. & Shaoqi, Z. 2020. Adsorption of methylene blue in water onto activated carbon by surfactant modification. *Water* 12(2): 587-606.

Kumar, P.V., Ahamed, A.J. & Karthikeyan, M. 2019. Synthesis and characterization of NiO nanoparticles by chemical as well as green routes and their comparisons with respect to cytotoxic effect and toxicity studies in microbial and MCF-7 cancer cell models. *SN Applied Sciences* 1(9): 1-5.

Lim, L.B.L. 2017. Breadnut peel as a highly effective low-cost biosorbent for methylene blue: Equilibrium, thermodynamic and kinetic studies. *Arabian Journal of Chemistry* 10: S3216-S3228.

Lingaraju, K., Naika, H.R., Nagabhushana, H., Jayanna, K., Devaraja, S. & Nagaraju, G. 2020. Biosynthesis of nickel oxide nanoparticles from *Euphorbia heterophylla* (L.) and their biological application. *Arabian Journal of Chemistry* 13(3): 4712-4719.

Mariam, A., Kashif, M. & Arokiyaraj, M. 2014. Bio-synthesis of NiO and Ni nanoparticles and their characterization. *Digest Journal of Nanomaterials and Biostructures* 9(3): 1007-1019.

Marzieh, R. & Rouhollah, H. 2014. Biosynthesis of silver nanoparticles using extract of olive leaf: Synthesis and *in vitro* cytotoxic effect on MCF-7 cells. *Journal of Nanostructure in Chemistry* 4(3): 112.

Miessya, W., Yoki, Y., Iman, A. & Dewangga, O.A. 2019. Synthesis of NiO nanoparticles via green route using *Ageratum conyzoides* L. leaf extract and their catalytic activity. In *IOP Conference Series: Materials Science and Engineering.* IOP. 012077.

Nagaraj, B., Krishnamurthy, N.B., Liny, P., Divya, T.K. & Dinesh, R. 2011. Biosynthesis of gold nanoparticles of *Ixora coccinea* flower extract & their antimicrobial activities. *International Journal of Pharma Bio Sciences* 2(4): 557-565.

Nasseri, M.A., Ahrari, F. & Zakerinasab, B. 2016. A green biosynthesis of NiO nanoparticles using aqueous extract of *Tamarix serotina* and their characterization and application. *Applied Organometallic Chemistry* 30(12): 978-984.

Olajire, A.A. & Mohammed, A.A. 2020. Green synthesis of nickel oxide nanoparticles and studies of their photocatalytic activity in degradation of polyethylene films. *Advanced Powder Technology* 31(1): 211-218.

Pandian, C.J., Palanivel, R. & Dhananasekaran, S. 2015. Green synthesis of nickel nanoparticles using *Ocimum sanctum* and their application in dye and pollutant adsorption. *Chinese Journal of Chemical Engineering* 23(8): 1307-1315.

Parveen, K., Banse, V. & Ledwani, L. 2016. Green synthesis of nanoparticles: Their advantages and disadvantages. In *AIP Conference Proceedings.* AIP. 020048.

Patel, K.J., Bhatt, G.G., Ray, J.R., Suryavanshi, P. & Panchal, C.J. 2017. All inorganic solid-state electrochromic devices: A review. *Journal of Solid State Electrochemistry* 21(2): 337-347.

Pelgrift, R.Y. & Friedman, A.J. 2013. Nanotechnology as a therapeutic tool to combat microbial resistance. *Advanced Drug Delivery Reviews* 65(13-14): 1803-1815.

Pooja, K. & Dipali, S. 2017. Synthesis and characterization of nickel oxide nanoparticles by using co- precipitation method. *International Journal of Advanced Research* 5(5): 1333-1338.

Pooyandeh, S., Shahidi, S., Khajehnezhad, A. & Ghoranneviss, Z. 2020. Synthesizing and deposition of nickel oxide nanoparticles on glass mat using sol-gel method (morphological and magnetic properties). *Journal of the Textile Institute* 112(6): 887-895.

Priyadarshini, B., Rath, P.P., Behera, S.S., Panda, S.R., Sahoo, T.R. & Parhi, P.K. 2018. Kinetics, thermodynamics and isotherm studies on adsorption of eriochrome Black-T from

aqueous solution using rutile TiO_2. In *IOP Conference Series: Materials Science and Engineering*. IOP. 012051.

Rahdar, A., Aliahmad, M. & Azizi, Y. 2015. NiO nanoparticles: Synthesis and characterization. *Journal of Nanostructure* 5(2): 145-151.

Raval, N.P., Shah, P.U. & Shah, N.K. 2016. Nanoparticles loaded biopolymer as effective adsorbent for adsorptive removal of malachite green from aqueous solution. *Water Conservation Science and Engineering* 1(1): 69-81.

Saiganesh, S., Krishnan, T. & Mallikarjuna, K. 2020. Phytogenic generation of NiO nanoparticles using stevia leaf extract and evaluation of their *in-vitro* antioxidant and antimicrobial properties. *Biomolecules* 10(1): 89.

Salvadori, M.R., Ando, R.A., Nascimento, C.A.O. & Corrêa, B. 2015. Extra and intracellular synthesis of nickel oxide nanoparticles mediated by dead fungal biomass. *PLoS ONE* 10(6): e0129799.

Serpil, S. & Mehmet, M.U. 2017. Adsorption of methylene blue and methyl orange by using waste ash. *Journal of Natural and Applied Sciences* 21(3): 831-835.

Shah, M., Fawcett, D., Sharma, S., Tripathy, S.K. & Poinern, G.E.J. 2015. Green synthesis of metallic nanoparticles via biological entities. *Materials* 8(11): 7278-7308.

Sonea, B.T., Manikandana, E., Gurib-Fakima, A. & Maazaa, M. 2016. Single-phase α-Cr_2O_3 nanoparticles' green synthesis using *Callistemon viminalis'* red flower extract. *Green Chemistry Letters and Reviews* 9(2): 85-90.

Sun, Bo., Jing-Bing, L., Hao, W. & Hui, Y. 2017. Application of nickel oxide nanoparticles in electronic materials. *Ionics* 23: 1509-1515.

Thema, F.T., Manikandan, E. & Ameenah, G. 2016. Single phase bunsenite NiO nanoparticles green synthesis by *Agathosma betulina* natural extract. *Journal of Alloys and Compounds* 657: 655-661.

Zorkipli, N.N.M., Kaus, N.H.M. & Mohamad, A.A. 2016. Synthesis of NiO nanoparticles through sol-gel method. *Procedia Chemistry* 19: 626-631.

Department of Biochemical Engineering
Al-Khwarizmi College of Engineering
University of Baghdad
Iraq

*Corresponding author; email: sami.albayati@gmail.com

Received: 17 February 2021
Accepted: 12 June 2021